

## Effect of substrate temperature on structural and electrical properties of non-stoichiometric In<sub>0.35</sub>Sb<sub>0.65</sub> thin films deposited by thermal evaporation

K. Shriram <sup>a,\*</sup>, A. Verma <sup>a</sup>, R. R. Awasthi <sup>b</sup>, B. Das <sup>a</sup>

<sup>a</sup> Department of Physics, University of Lucknow, Lucknow-226007, U.P., India

<sup>b</sup> Faculty of Engineering and Technology, Khwaja Moinuddin Chisti Language University, Lucknow- 226013, Uttar India

This study investigated the effects of substrate temperature on the structural and electrical properties of non-stoichiometric In<sub>0.35</sub>Sb<sub>0.65</sub> thin films fabricated using thermal evaporation. Films with a constant thickness of 450 nm were deposited on glass substrates at temperatures ranging from 300 to 383 K. X-ray diffraction analysis revealed polycrystalline films with a zinc-blende structure predominantly oriented along the (220) and (311) planes. As the substrate temperature increased, the crystallite size decreased from 29 nm to 21 nm, while the line strain and dislocation density increased. Electrical characterization confirmed the p-type semiconductivity in all films. The resistivity increased from 0.282 Ω-cm to 19.3 Ω-cm with increasing substrate temperature. Notably, the hole mobility significantly improved from 730 cm<sup>2</sup>/V-s to 44,400 cm<sup>2</sup>/V-s, which is attributed to the reduced grain boundary scattering at higher deposition temperatures. Conversely, the carrier concentration decreased from 3.04×10<sup>16</sup> cm<sup>-3</sup> to 7.96×10<sup>12</sup> cm<sup>-3</sup> as the temperature increased. These findings demonstrate the substantial influence of the substrate temperature on the structural and electrical properties of thermally evaporated InSb thin films, providing insights for optimizing their performance in various applications.

(Received April 4, 2025; Accepted June 6, 2025)

*Keywords:* Thin film, Mobility, Grain

### 1. Introduction

In a previous study, we characterized p-type InSb thin films of different thicknesses. X-ray diffraction patterns and scanning electron microscopy revealed that the grain size, dislocation density, and strain varied with the thickness of the thin films. The Hall measurement, four probes, and UV-Vis NIR show the variation in carrier concentration, carrier mobility, resistivity, and optical band gap with the change in thickness. In the present chapter, we fabricated non-stoichiometric In<sub>0.35</sub>Sb<sub>0.65</sub> thin films with different substrate temperatures (300 K -383 K) and 450 nm thicknesses. The structural and electrical properties of semiconducting thin films are highly dependent on their deposition temperatures. Owing to their structures, III–IV semiconductors play a major role in scientific research and applications. Among the III-IV binary compound semiconductors, indium antimonide (InSb) exhibits p-type and n-type semiconductivity [1]. Devices made of indium antimonide semiconductors can function at voltages as low as 0.5 V, which minimizes their power consumption. High-mobility photodetectors in the long-wavelength infrared (LWIR) and mid-wavelength infrared (MWIR) regions, single-crystal InSb, and InAs<sub>1-x</sub>Sb<sub>x</sub> have also been used [2], [3]. One of the most investigated binary III-V compounds is InSb, which has the highest hole and electron mobilities among all semiconductors at room temperature (1250 cm<sup>2</sup> V<sup>-1</sup> s and 10,240 cm<sup>2</sup> V<sup>-1</sup> s) [4]. Owing to its high electron and hole mobility, it is an essential semiconductor for the development of infrared detectors in the 3-5 μm wavelength region, as well as in electronic and optoelectronic devices [5], [6]. Because of their excellent carrier mobility, low effective mass, and large g-factor, low-dimensional high-quality InSb materials are promising candidates for next-generation quantum devices [7]. Antimony-rich thin-

---

\* Corresponding author: rs2018phy\_kartikey@lkouniv.ac.in  
<https://doi.org/10.15251/JOBM.2025.172.109>

film materials exhibit p-type semiconducting behavior, whereas indium-rich thin-film materials exhibit n-type semiconducting behavior. N-type InSb thin films can also be used as bacterial biosensors [8]. Owing to its unique features, InSb has applications in high-speed transistors, magnetoresistance, speed-sensitive sensors, and Hall sensors [5]. InSb p-n junctions have 100% internal quantum efficiency and exhibit photovoltaic effects under infrared light [9]. Molecular beam epitaxy, flash evaporation [10], sputtering [11], vacuum evaporation [12], electrospinning [13], chemical oxidative polymerization [14], and chemical and ultrasonic treatment methods [15] [16][17] a few growth techniques.

Revathi et al. investigated the physical properties of  $\text{In}_2\text{S}_3$  films deposited on glass substrates via closely spaced evaporation at various temperatures (200-350°C). They analyzed the chemical composition, structure, surface morphology, and optical and electrical properties of the films. The films were sulfur-rich at lower temperatures and indium-rich at higher temperatures. Optimal stoichiometry was achieved at 300°C. The films exhibited both cubic and tetragonal  $\beta$ - $\text{In}_2\text{S}_3$  phases at low temperatures, with a predominantly tetragonal phase observed at 350°C. The grain size increased from 10 to 32 nm as the temperature increased from 200 to 300°C, and then decreased to 23 nm at 350°C. The transmittance increased with temperature, peaking at 78% for the films deposited at 300°C. The optical band gap increased from 2.09 to 2.52 eV with increasing temperature up to 300°C. The conductivity increased with increasing temperature up to 300°C, and then decreased. Two distinct conduction mechanisms are observed: thermionic emission at higher temperatures and Mott hopping at lower temperatures. This study demonstrated that substrate temperature significantly influences the physical properties of  $\text{In}_2\text{S}_3$  films, with optimal characteristics generally achieved at 300°C [18]. Yildiz et al. investigated the relationship between the substrate temperature and electrical properties of titanium dioxide thin films deposited by DC sputtering. They found that the electrical resistivity decreased with increasing substrate temperature owing to improved crystallinity and larger crystallite sizes. Three conduction mechanisms were identified in different temperature ranges: grain boundary scattering (>150 K), nearest-neighbor hopping (55-150 K), and variable range hopping (<55 K). The authors analyzed these mechanisms using various models and determined parameters such as barrier height, donor concentration, and density of states at the Fermi level. They observed that higher substrate temperatures led to increased donor concentrations and decreased compensation ratios, resulting in a lower resistivity. This study provides insights into the effects of substrate temperature on the electrical properties of  $\text{TiO}_2$  thin films, which could be valuable for developing electronic devices based on this material [19]. Jassim et al. investigated the influence of substrate temperature on CdS thin films deposited by thermal evaporation. They prepared films at 20, 100, and 200°C and analyzed their structural, optical, and electrical properties. X-ray diffraction revealed polycrystalline films with a hexagonal wurtzite structure, preferentially oriented along the (002) plane. The film thickness decreased from 1600 nm to 200 nm as the substrate temperature increased. Optical transmittance exceeded 80% in the visible range, with band gap values between 2.3-2.43 eV, decreasing with higher substrate temperatures. The electrical conductivity was low, ranging from  $3.2 - 22 (\Omega \text{ cm})^{-1}$ , increasing as the substrate temperature decreased. The authors concluded that these CdS films, with their wide bandgap and high optical transparency, could be suitable as window layers in solar cells [20]. Ghorannevis et al. investigated the effects of the substrate temperature on Al-doped ZnO (Al/ZnO) thin films deposited using DC magnetron sputtering. They examined the structural, morphological, and optical properties of the films at different substrate temperatures (150-350°C). X-ray diffraction analysis revealed that crystallinity depended on the substrate temperature. SEM and AFM analyses showed an increased grain size and surface roughness at higher temperatures. The film thickness also increased with temperature, as confirmed by surface profiler measurements. Optical transmission spectra indicated high transparency (>90%) in the visible region, with band gap energies increasing from 3.33 to 3.38 eV as substrate temperature rose. The authors concluded that the substrate temperature significantly influences the growth behavior and properties of Al/ZnO thin films, affecting their potential applications in optoelectronic devices [21]. Reddy et al. investigated the temperature-dependent optical properties of gold thin films, focusing on single and polycrystalline samples with thicknesses ranging from 30 nm to 200 nm. They measured optical constants at elevated temperatures (up to 500°C) using variable-angle spectroscopic ellipsometry. The study revealed

that while the real part of the dielectric function changed marginally with increasing temperature, the imaginary part changed significantly. For the 200-nm-thick films, the imaginary part at 500°C was nearly twice as large as that at room temperature. In thinner films (50-nm and 30-nm), the imaginary part showed both increasing and decreasing behavior depending on the temperature range, ultimately becoming to 3-4 times larger at 500°C than at room temperature. The authors provided experimentally fitted models to describe the temperature-dependent gold dielectric function using the Drude and two critical-point oscillator models. These findings have important implications for high-temperature plasmonic and near-field radiative heat transfer applications [22]. Fang et al. investigated the influence of the substrate temperature on the properties of erbium-doped aluminum nitride (AlN: Er) films deposited via reactive radio-frequency magnetron sputtering. This study examined films prepared at temperatures ranging from unintentionally heated to 400°C. XPS analysis revealed uniform Er<sup>3+</sup> doping of the AlN films. FESEM revealed dense, compact columnar structures regardless of the substrate temperature. AFM measurements indicated the lowest surface roughness ( $6.1 \pm 1.0$  nm) for films deposited at 300°C. The GIXRD patterns were explained using the hexagonal wurtzite AlN crystallography. Williamson-Hall analysis showed the largest crystallite size (~28 nm) for films deposited at 300°C. The strongest room-temperature photoluminescence was observed for the films deposited at 300°C. The authors concluded that 300°C is the optimal substrate temperature for AlN: Er film deposition when prioritizing photoluminescence intensity. However, lower temperatures may be suitable for heat-sensitive metal components, albeit with reduced luminescence [23]. Kouidri et al. investigated the properties of cobalt oxide (Co<sub>3</sub>O<sub>4</sub>) thin films deposited on glass substrates using spray pyrolysis at different temperatures (250-450°C). The films exhibited a polycrystalline cubic spinel structure, with the preferred orientation shifting from (311) to (111) with an increase in temperature. The morphological analysis revealed homogeneous and well-covered surfaces. The optical transmittance improved with higher substrate temperatures, and two direct band gaps ( $E_{g1}$ : 1.444-1.495 eV,  $E_{g2}$ : 1.969-2.093 eV) were observed. The electrical conductivity increased from  $6.684 \times 10^{-4}$  to  $1.623$  ( $\Omega$  cm)<sup>-1</sup> with increasing temperature, reaching a maximum value at 400°C. The authors concluded that the prepared Co<sub>3</sub>O<sub>4</sub> films exhibited properties suitable for various applications, including supercapacitor electrodes [24]. Das et al. investigated the effect of the substrate temperature on CdS thin films deposited by RF sputtering for solar cell applications. They found that increasing the substrate temperature from 25 to 300°C improved the film crystallinity, with a hexagonal wurtzite structure oriented along the (002) plane. At higher temperatures, the crystallite size increases, whereas the microstrain and dislocation density decrease. The films showed high optical transmittance (75-90%) and a decreasing bandgap (2.34-2.26 eV) with temperature. Electrical properties improved, with resistivity decreasing from 2.77 to 0.93 k $\Omega$ -cm and mobility increasing from 5.53 to 12.57 cm<sup>2</sup>/V-s as temperature increased. The authors concluded that the films deposited at 300°C had the most suitable properties for use as window layers in thin-film solar cells [25].

## 2. Material and methods

### 2.1. Fabrication of p-type InSb thin films of different substrate temperature

Non-stoichiometric p-InSb thin films with different substrate temperatures (300 K-383 K) were deposited by thermal evaporation on a clean glass substrate using the source material composition In<sub>0.35</sub>Sb<sub>0.65</sub> in vacuum kept below 10<sup>-5</sup> torr. The source material was kept in a molybdenum boat, the heated filament was supplied by an L T power supply in a vacuum chamber, and the vacuum was kept below 10<sup>-5</sup> torr in a vacuum coating unit. The distance between the substrate and source material was maintained at 12 cm for all depositions. Approximately 40 mg of source material was used for the deposition of each thin film. In each deposition cycle, fresh source material was kept in a molybdenum boat. The evaporated particles in vapor form from the evaporant material were deposited on a glass substrate in thin film form. The fabricated thin films were cooled under the same vacuum pressure. During the deposition of the thin film, the substrate was placed normal to the line of sight from the evaporation surface at different polar angles to obtain uniform deposition. The thickness and deposition rate of the thin films were measured using

a digital film thickness monitor (FDTM 10) with a quartz sensor set at 6 MHz. The sensor of the film thickness monitor was attached parallel to the substrate holder and at the same distance from the evaporant source material. The rate of film deposition was kept constant during the fabrication of the thin films and was controlled by the applied current. The substrate temperature was measured in a vacuum chamber using a digital temperature meter (Nutronics PTC 201) attached to a thermocouple sensor. The tip of the thermocouple sensor was placed at a constant position on the surface of the substrate. The p-type InSb thin films were structurally and electrically characterized using GIXRD and Hall measurements. The variation in the structural and electrical parameters with the film deposition temperature was studied.

### 3. Result and discussion

#### 3.1. Structural characterization of the fabricated thin films

The GIXRD patterns of the p-type InSb thin films were recorded using a Panalytical X'Pert Pro X-ray diffractometer using  $\text{Cu}_{\alpha 1}$  with a wavelength  $\lambda=1.5406 \text{ \AA}$  with a Ni-filer at 45 KV and 40 mA. The X-ray source was fixed at  $1^\circ$  and the scanning angle was fixed at  $20^\circ\text{--}60^\circ$ . A diffractometer was used to record data. The X-ray diffractogram of the p-type InSb thin films is presented in Section 1. Thin films were prepared using the source/bulk material  $\text{In}_{0.35}\text{Sb}_{0.65}$  at different substrate temperatures. These XRD patterns reveal that the p-type InSb thin films are polycrystalline and have Zincblende Structures. The thin films were oriented along the (220) and (311) planes.

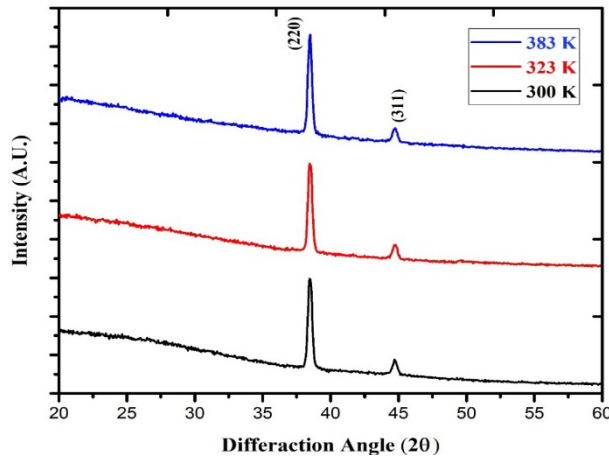


Fig. 1. GIXRD patterns of p-type InSb thin film with different substrate temperature.

#### 3.2. Calculation of structural parameter of p-type InSb thin films

The crystallite sizes ( $D$ ) of the p-type InSb thin films were calculated using the Debye-Scherrer equation, as shown in Table 1.

$$D = \left( \frac{0.94\lambda}{\beta \cos \theta} \right) \quad (1)$$

where  $\beta$  is the FWHM of the diffraction peak,  $\lambda$  is the X-ray wavelength, and  $\theta$  is the diffraction angle.

The strain ( $\varepsilon$ ) for p-type InSb thin films was calculated using the following relationship, and is presented in Table 1.

$$\beta \cos \theta = \frac{K\lambda}{D} + 4\varepsilon \sin \theta \quad (2)$$

The dislocation density ( $\delta$ ) is defined as the length of dislocation line per unit volume of the crystal and its value is calculated with the help of crystallite size (D) for the p-type InSb thin films, using the following formula and calculated value given in the Table -1

$$\delta = \frac{n}{D^2} \quad (3)$$

The lattice constant 'a' calculated for crystals of p-type InSb thin films with the help of the (311) plane and the following equation is shown in Table 5.1.

$$a = (d)\sqrt{(h^2 + k^2 + l^2)} \quad (4)$$

where 'd' is interplanar space and h, k, l are Miller indices.

The XRD patterns showed that the crystallites had a zincblende structure with orientations along the (220) and (311) planes. It has been observed in earlier studies that the intensity of diffraction peaks increases with an increase in substrate temperature. The crystallite sizes (D) of p-type InSb thin films with different substrate temperatures and thicknesses of 450 nm are listed in Table 1. As shown in Table 1, the crystallite size (D) decreased from 29 to 21 nm when the substrate temperature increased from 300 K to 383 K. The substrate temperature 300 K of resulted in the largest crystallite size of 29 nm. The strains of p-type InSb thin films fabricated at substrate temperatures ranging from 300 to 383 K using diffraction patterns are listed in Table 1. The line strain increased by  $3.688 \times 10^{-3} \text{ Line}^{-2}\text{m}^{-4} - 4.306 \times 10^{-3} \text{ Line}^{-2}\text{m}^{-4}$  with an increase in the substrate temperature. The dislocation density of p-type InSb thin films increased from  $1.1282 \times 10^{15} \text{ line/m}^2$  to  $2.139 \times 10^{15} \text{ line/m}^2$  with increasing substrate temperature. A minimum dislocation density of  $1.1282 \times 10^{15} \text{ line/m}^2$  was observed for a film with a thickness of 450 nm and substrate temperature of 300 K.

Table 1. Structural parameter of p-type InSb thin films fabricated at different substrate temperature.

SUBSTRATE TEMP.	Crystallite Size (nm)	Dislocation Density $10^{15} \text{ line/m}^2$	Lattice parameter (Å)	Strain ( $\epsilon$ ) $\text{Line}^{-2}\text{m}^{-4}$
S1 (300 K)	29	1.1282	6.6090924	0.003688
S2 (323 K)	25	1.5355	6.6088125	0.0043033
S3 (383 K)	21	2.1393	6.59384845	0.0043068

### 3.2.1. Electrical characterization of p-type InSb thin films

The electrical characterization of these non-stoichiometric InSb thin films was performed by measuring the electrical resistivity and Hall parameters. The resistivity of the films was determined by four-probe resistivity measurements. Hall measurements provide information about the type of charge carriers in semiconducting thin films and the Hall coefficient, carrier concentration, and carrier mobility. The Hall parameters are the most important parameters for semiconductors. The carrier concentration and Hall mobility of the thin films were calculated using the ratio of the Hall coefficient to the electrical resistivity, which were measured using Hall measurements and the four-probe technique, respectively.

### 3.2.2. Electrical analysis of p-type InSb thin films

The electrical resistivities and activation energies of films deposited at different substrate temperatures are listed in Table 2. The Hall coefficients, carrier concentrations, and Hall mobilities of the films are listed in Table 2. These measurements were performed on InSb thin films with a thickness of 450 nm at room temperature. Hall measurements revealed that the films exhibited a p-type semiconductivity.

Table 2. Electrical properties of p-type InSb thin film with different substrate temperature.

Substrate Temperature	Resistivity ( $\Omega$ -cm)	Sheet Resistance ( $\Omega$ /sq)	Sheet carrier concentration ( $\text{Cm}^{-2}$ )	Bulk carrier concentration ( $\text{Cm}^{-3}$ )	$R_H$ ( $\text{Cm}^3/\text{C}$ )	Mobility ( $\text{Cm}^2/\text{V-s}$ )
S1 (300 K)	2.82E-01	6.26E+03	1.37E+12	3.04E+16	2.06E+02	7.30E+02
S2 (323 K)	1.77E+01	3.92E+05	4.67E+09	1.04E+14	6.01E+04	3.12E+03
S3 (383 K)	1.93E+01	4.29E+05	3.58E+08	7.96E+12	7.84E+05	4.44E+04

### 3.2.3. Resistivity of p-type InSb thin films

The electrical resistivities of the non-stoichiometric p-type InSb thin films measured at room temperature for fabrication at different substrate temperatures are listed in Table 2. The variations in electrical resistivity at different substrate temperatures are shown in Figure 2. It is found from Figure 5.2 that the electrical resistivity of these thin films increases from 0.282 ohm-cm – to 19.3 ohm-cm with a change of film fabrication temperature. The minimum electrical resistivity of 0.282  $\Omega$  cm was observed for a thin film with a thickness of 450 nm fabricated at 300 K.

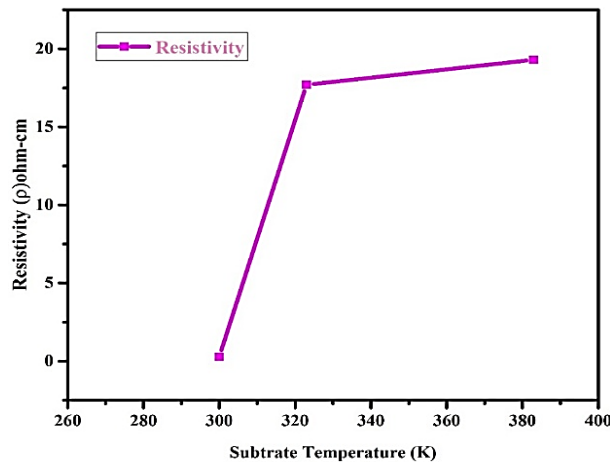


Fig. 2. Variation of thin film resistivity ( $\rho$ ) with different substrate temperature.

### 3.2.4. Carrier mobility of p-type InSb thin film

The carrier mobility of p-type non-stoichiometric InSb fabricated at different substrate temperatures (300 K-383K) measured at room temperature with the  $\text{In}_{0.35}\text{In}_{0.65}$  composition of the source material is listed in Table 2. The variation in the hole mobility of p-type InSb thin films fabricated at different temperatures of indium antimonide (InSb) is shown in Figure 3. Hall measurements revealed that the films exhibited p-type semiconductivity. As shown in Figure 3, the

hole mobility ( $\mu_h$ ) in p-type InSb thin films increased by  $730 \text{ cm}^2 / \text{V-s} - 44,400 \text{ cm}^2/\text{V-s}$  with a change in the substrate temperature of the thin films owing to the decrease in grain boundary scattering. A maximum hole mobility of  $44,400 \text{ cm}^2/\text{V-s}$  was observed for a p-type InSb thin film prepared using the source/bulk material with a composition of  $\text{In}_{0.35}\text{Sb}_{0.65}$ , with a thickness of 450 nm. This indicates that the crystals grown in p-type InSb thin films at this temperature are larger than those of the films fabricated at all temperatures.

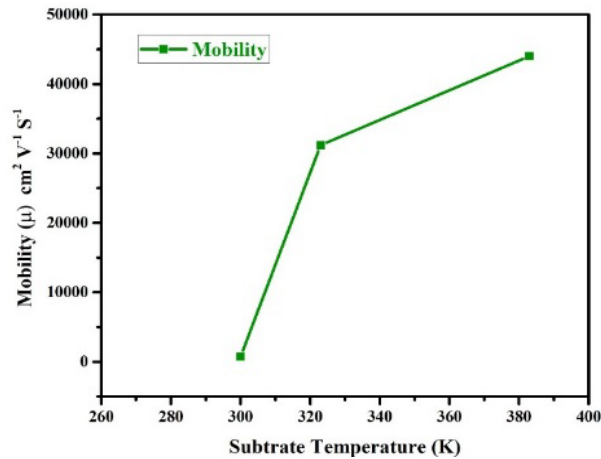


Fig. 3. Variation of carrier mobility ( $\mu$ ) with different substrate temperature.

### 3.2.5. Carrier concentration of p-type InSb thin films

The carrier concentrations of non-stoichiometric p-type InSb thin films of indium antimonide fabricated at different substrate temperatures (300 K-383K) were calculated using the Hall coefficient, and the results are presented in Table 2. The variation in the carrier concentration in the p-type InSb thin film as a function of the substrate temperature is shown in Figure 4. As shown in Figure 4, the carrier concentration in p-type InSb thin films decreases as the substrate temperature 300 K-380 K from  $3.04 \times 10^{16} \text{ cm}^{-3}$  to  $7.96 \times 10^{12} \text{ cm}^{-3}$ . The carrier concentration in the thin film was affected by the parallel conduction at the surface.

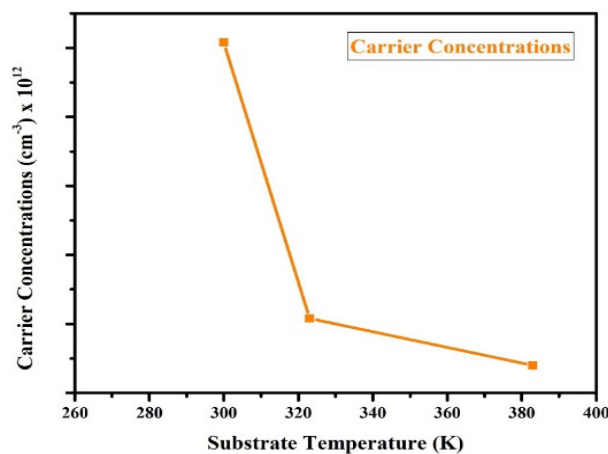


Fig. 4. Variation of Carrier concentration with different substrate temperature.

#### 4. Conclusion

In this study, non-stoichiometric InSb thin films were successfully fabricated using a thermal evaporation technique. The films were deposited on glass substrates at temperatures ranging from 300 to 383 K with a thickness of 450 nm using  $\text{In}_{0.35}\text{Sb}_{0.65}$  as the bulk/source material. X-ray diffraction analysis revealed that the deposited films were polycrystalline with a zinc-blende structure that was predominantly oriented along the (220) and (311) planes. Structural characterization showed that the crystallite size decreased from 29 nm to 21 nm as the substrate temperature increased from 300 K to 383 K. Conversely, the line strain and dislocation density increased with increasing substrate temperature, indicating a deterioration in the crystal quality at higher deposition temperatures. The electrical characterization confirmed the p-type semiconductivity of the films. The resistivity of the films increased from 0.282  $\Omega\text{-cm}$  to 19.3  $\Omega\text{-cm}$  with increasing substrate temperature. Notably, the hole mobility increased significantly from 730  $\text{cm}^2/\text{V-s}$  to 44,400  $\text{cm}^2/\text{V-s}$  as the substrate temperature increased. This improvement in mobility was attributed to the reduced grain boundary scattering in the films deposited at higher temperatures. However, the carrier concentration exhibited an inverse relationship with the substrate temperature, decreasing from  $3.04 \times 10^{16} \text{ cm}^{-3}$  to  $7.96 \times 10^{12} \text{ cm}^{-3}$  as the temperature increased from 300 K to 383 K. This decrease may have been influenced by the surface-related parallel conduction effects. These findings demonstrate the significant impact of the substrate temperature on the structural and electrical properties of thermally evaporated InSb thin films. The ability to control these properties by varying the deposition temperature offers a pathway for optimizing the InSb thin films for various applications in electronic and optoelectronic devices.

#### References

- [1] S R Vishwakarma, A K Verma, R S N Tripathi, S Das, Rahul, Indian J Pure & Applied Phys, 50, 346 (2012).
- [2] A. Rogalski, P. Martyniuk, M. Kopytko, P. Madejczyk, and S. Krishna, Sensors, 20 1 (2020); <https://doi.org/10.3390/s20247047>
- [3] A. Karim, J. Y. Andersson, Materials Science and Engineering, 51 012001 (2013); <https://doi.org/10.1088/1757-899X/51/1/012001>
- [4] K. E. Hnida et al., J Mater Chem C Mater, 4 1345 (2016); <https://doi.org/10.1039/C5TC03656A>
- [5] J. Heremans, D. L. Partin, C. M. Thrush, L. Green, Semicond. Sci. Technol 8 424 (1993); <https://doi.org/10.1088/0268-1242/8/1S/093>
- [6] T. Ashley, A. B. Dean, C. T. Elliott, G. J. Pryce, A. D. Johnson, H. Willis, Appl Phys Lett, 66 481 (1995); <https://doi.org/10.1063/1.114063>
- [7] S. Gazibegovic et al. Advanced Materials, 31 14 (2019); <https://doi.org/10.1002/adma.201808181>
- [8] H. D. Park, S. M. Prokes, M. E. Twigg, Y. Ding, Z. L. Wang, J Cryst Growth, 304 399 (2007); <https://doi.org/10.1016/j.jcrysgro.2007.03.023>
- [9] T. Miyazaki, S. Adachi, J Appl Phys, 70 1672 (1991); <https://doi.org/10.1063/1.349535>
- [10] C. K. Sumesh, K. D. Patel, G. K. Solanki, V. M. Pathak, R. Srivastav, EPJ Applied Physics, 54 1 (2011); <https://doi.org/10.1051/epjap/2011100484>
- [11] T. Miyazaki, M. Kunugi, Y. Kitamura, S. Adachi, Journal of Applied Physics, 70 1672 (1991); <https://doi.org/10.1063/1.349535>
- [12] M. Tomisu, N. Lnoue, Y. Yasuoka, Vacuum 47 239 (1996); [https://doi.org/10.1016/0042-207X\(95\)00208-1](https://doi.org/10.1016/0042-207X(95)00208-1)
- [13] K. R. Reddy, V. G. Gomes, M. Hassan, Mater Res Express, 1 1 (2014); <https://doi.org/10.1088/2053-1591/1/1/015012>
- [14] K. R. Reddy, K. P. Lee, A. I. Gopalan, J Appl Polym Sci, 106 1181 (2007);

<https://doi.org/10.1002/app.26601>

[15] K. R. Reddy, K. P. Lee, A. I. Gopalan, *Colloids Surf A Physicochem Eng Asp*, 320 49 (2008); <https://doi.org/10.1016/j.colsurfa.2007.12.057>

[16] K. R. Reddy, K. V. Karthik, S. B. B. Prasad, S. K. Soni, H. M. Jeong, A. V. Raghu, *Polyhedron*, 20 169 (2016); <https://doi.org/10.1016/j.poly.2016.08.029>

[17] K. R. Reddy, K. Nakata, T. Ochiai, T. Murakami, D. A. Tryk, A. Fujishima, *Journal of Nanoscience and Nanotechnology* 11 3692 (2011); <https://doi.org/10.1166/jnn.2011.3805>

[18] N. Revathi, P. Prathap, Y. P. V. Subbaiah, K. T. R. Reddy, *J Phys D Appl Phys*, 41 15 (2008); <https://doi.org/10.1088/0022-3727/41/15/155404>

[19] A. Yildiz, S. B. Lisesivdin, M. Kasap, D. Mardare, *Journal of Materials Science: Materials in Electronics*, 21 7, 692-697, (2010); <https://doi.org/10.1007/s10854-009-9979-z>

[20] S. A. J. Jassim, A. A. R. A. Zumaila, G. A. A. Al Waly, *Results Phys*, 3 173-178 (2013); <https://doi.org/10.1016/j.rinp.2013.08.003>

[21] Z. Ghorannevis, M. T. Hosseinnejad, M. Habibi, P. Golmahdi, *Journal of Theoretical and Applied Physics*, 9 1, 33-38, (2015); <https://doi.org/10.1007/s40094-014-0157-1>

[22] H. Reddy, U. Guler, A. V. Kildishev, A. Boltasseva, V. M. Shalaev, *Opt Mater Express*, 6 9 2776 (2016); <https://doi.org/10.1364/OME.6.002776>

[23] L. Fang et al, *Materials*, 11 11 (2018); <https://doi.org/10.3390/ma11112196>

[24] N. Kouidri, S. Rahmane, A. Allag, *Journal of Materials Science: Materials in Electronics*, 30 2 1153-1160, (2019); <https://doi.org/10.1007/s10854-018-0384-3>

[25] N. K. Das et al. *Results Phys* 17 (2020); <https://doi.org/10.1016/j.rinp.2020.103132>